NJC

Alkyl-functionalization of 3,5-bis(2-pyridyl)-1,2,4,6-thiatriazine

Journal:	*New Journal of Chemistry*
Manuscript ID	NJ-ART-09-2015-002611.R2
Article Type:	Paper
Date Submitted by the Author:	13-Jan-2016
Complete List of Authors:	Kleisath, Elizabeth; University of Ottawa, Chemistry Yutronkie, Nathan; University of Ottawa, Chemistry Korobkov, Ilia; University of Ottawa, Department of Chemistry Gabidullin, Bulat; University of Ottawa, Department of Chemistry Brusso, Jaclyn; University of Ottawa, Department of Chemistry

New Journal of Chemistry

ARTICLE

Alkyl-functionalization of 3,5-*bis*(2-pyridyl)-1,2,4,6-thiatriazine

Elizabeth Kleisath,[ab] Nathan J. Yutronkie,[ab] Ilia Korobkov,[a] Bulat M. Gabidullin[a] and Jaclyn L. Brusso*[ab]

Received 00th January 20xx,
Accepted 00th January 20xx

DOI: 10.1039/x0xx00000x

www.rsc.org/njc

A versatile synthetic route to prepare alkyl functionalized 3,5-*bis*-(2-pyridyl)-1,2,4,6-thiatriazines is described that can proceed either *via* cationic or anionic pathways; confirmed through characterization of the isolable intermediates. Computational studies are presented, which support the regioselectivity of the alkylation reactions and photophyscial properties of the *S*-alkylated derivatives.

Introduction

In recent years, the design and development of sulphur and nitrogen based heterocycles has received much attention due in large part to their suitability in a variety of applications.[1-6] In that regard, 1,2,4,6-thiatriazines (TTA) represent an important class of S-N heterocycles that have been explored as building blocks in the development of molecular conductors,[7-10] in addition to their use as spin bearing ligands in transition metal and lanthanide complexes.[11-14] Encouraged by the accessibility of both the oxidized (TTA^+) and reduced (TTA^-) forms of TTA,[15] we are interested in exploring its potential towards functionalization post TTA ring formation. The generation of a flexible and general route that enables modification of the exocyclic substituents holds significant potential in the design of novel heterocyclic compounds that can be targeted for a variety of applications such as mesogens in liquid crystalline materials, ionic liquids or electroactive substrates, in addition to their implementation as biologically active materials, namely in herbicidal applications.[16-19] Inclusion of heterocycles at the 3- and 5-position of the TTA ring that contain nitrogen, oxygen or sulfur facilitates the development of chelating ligands. This, in combination with substituents attached to the S atom can lead to novel systems in which multimetallic coordination complexes, polymers and extended networks can be envisioned. While thiatriazines functionalized at the 3- and 5-position of the TTA ring are well known,[11-13] only recently have heteroaromatic substituted TTA derivatives been reported (e.g., **1** where Ar = thienyl, pyridyl; Chart 1).[20] To that end, **1** (Ar = pyridyl) is an ideal candidate to explore in this study, as the heteroaromatic substituents are expected to promote coordination through the chelating effect rendering the N-S-N portion of the heterocyclic ring available for modification.

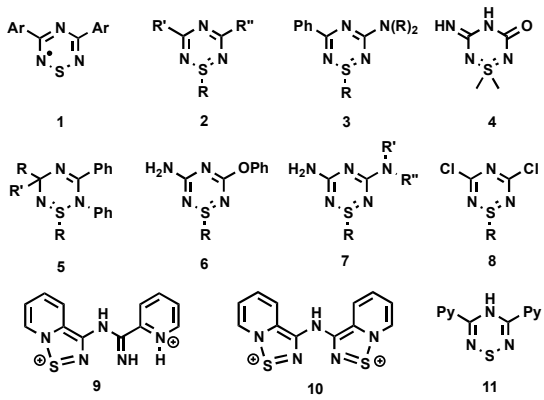

Chart 1. Examples of 1,2,4,6-thiatriazinyl radicals (**1**), *S*-alkyl-1,2,4,6-thiatriazine derivatives (**2**-**8**), *mono*- and *bis*-*N*-bridgehead-1,2,5-thiadiazolium salts (**9**, **10**) and **Py_2TTAH** (**11**).

With respect to heteroatom functionalization, examples of *S*-alkylated TTA rings have been reported (**2** – **8**). For the most part, such functionalization requires alkylation of the sulphur atom prior to TTA ring formation.[21-26] The one exception to this is **7**, where alkylation occurs *via* nucleophilic addition to 1,3,5-trichloro-1,2,4,6-thiatriazine in an S_N2 fashion.[27] Although shown to be effective, the latter route requires the generation of an *S*-chloro-1,2,4,6-thiatriazine. In the case of **1** (Ar = pyridyl), its synthesis involves the intermediacy of *mono*- and *bis*-*N*-bridgehead-1,2,5-thiadiazolium salts **9** and **10**, instead of the preparation of an *S*-chloro-1,2,4,6-thiatriazine.[28] This unique behaviour is attributed to the proclivity of the pyridyl moieties to form *N*-bridgehead-heterocycles, which enables the isolation of 3,5-*bis*(2-pyridyl)-4-hydro-1,2,4,6-thiatriazine (**Py_2TTAH**; **11**), a surprisingly robust compound with a high tolerance towards aqueous, basic, and thermal conditions. Since the N-S-N portion of the TTA ring in **Py_2TTAH** is devoid of substituents, we are currently exploring its potential towards functionalization, alkylation in particular. As a first step towards

[a] *Department of Chemistry and Biomolecular Sciences, University of Ottawa, 10 Marie Curie, Ottawa, Ontario K1N 6N5, Canada. E-mail: jbrusso@uottawa.ca*
[b] *Centre for Catalysis Research and Innovation, University of Ottawa, Ottawa, Ontario,K1N 6N5, Canada.*

Electronic Supplementary Information (ESI) available: NMR spectroscopy, crystallography, optical characterization and computational data. CCDC 1427397-1427399 and 1440653. See DOI: 10.1039/x0xx00000x

employing **Py_2TTAH** in an alternative synthetic route that facilitates modification of the exocyclic substituents, we herein report the synthesis and characterization of 3,5-*bis*(2-pyridyl)-*S*-methyl-1,2,4,6-thiatriazine (***S*-methyl-Py_2TTA**) and 3,5-*bis*(2-pyridyl)-*S*-ethyl-1,2,4,6-thiatriazine (***S*-ethyl-Py_2TTA**). Depending on the preparative route and alkylating agent employed, the *S*-alkylation can proceed through either cationic or anionic intermediates, which have been isolated and characterized. Computational studies were also carried out in order to probe the photophyscial properties of the *S*-alkylated derivatives and rationalize the regioselective alkylation. Overall, this work demonstrates an alternative and versatile synthetic route for post-functionalization of TTA rings, which can be achieved *via* two pathways.

Results and Discussion

Synthesis of *S*-alkyl-TTA derivatives *via* two pathways

Encouraged by the robustness of **Py_2TTAH**,[28] we sought to explore its potential towards functionalization. To that end, we considered direct alkylation using common alkylating reagents such as triethyloxonium tetrafluoroborate ($[Et_3O][BF_4]$), methyl triflate (MeOTf) and alkyl iodides (RI). Initial attempts involved the treatment of **Py_2TTAH** with $[Et_3O][BF_4]$ in dichloromethane (DCM), which afforded a mixture of purple needles and yellow block-like crystals. The purple needles, which were confirmed to be unreacted starting material, could easily be removed due to the solubility of **Py_2TTAH** in a variety of organic solvents. The resulting yellow block-like crystals were suitable for X-ray analysis (Figure 1), confirming the structural identity of **[*S*-ethyl-Py_2TTAH][BF_4]** (**12**, Scheme 1). Considering the TTA framework, the differences observed in the C—N bond lengths suggest discrete single and double bonds (Table S2), indicative of anti-aromatic character. This, coupled with the N—H signal observed in the IR and ^{1}H NMR spectra (Figure S1), as well as the presence of BF_4^- anions in the asymmetric unit, confirms **12** is the ionic species **[*S*-ethyl-Py_2TTAH][BF_4]**. The neutral compound ***S*-ethyl-Py_2TTA** (**14**) was isolated as a yellow solid *via* deprotonation of **12** with NaH, followed by aromatization. Recrystallization from hexanes afforded lustrous yellow needles of **14** suitable for structural analysis, the results of which are shown in Figure 1. Here, the six membered TTA ring adopts a shallow boat-like conformation with the S1 and N3 atoms deviated from the mean plane of the remaining four atoms by 0.402(1) Å and 0.074(2) Å, respectively. The relatively uniform C—N bond lengths in the TTA ring (see Table S2) is indicative of aromatic character, which is consistent with the expected six π-electron system. The molecular framework of ***S*-ethyl-Py_2TTA** is twisted with torsion angles of 12.8(1)° and 6.4(1)° between the pyridyl rings and the central TTA (Figure S14), with the C6 atom of the exocyclic ethyl substituent linked pseudo-axially.

Following a similar route, ***S*-methyl-Py_2TTA** (**15**) can be prepared. More specifically, the reaction of **Py_2TTAH** with MeOTf in DCM affords **[*S*-methyl-Py_2TTAH][OTf]** (**13**) as an iridescent white powder in 90 % yield. Comparison of the IR and NMR spectra of **[*S*-methyl-Py_2TTAH][OTf]** with **[*S*-ethyl-Py_2TTAH][BF_4]** reveal several similarities with the most significant differences attributed to the anion stretching frequencies in the IR spectra. For the ^{1}H NMR spectra, signals corresponding to the N—H and pyridyl protons overlap (Figure S1 and S2), while the methyl peak for the **[*S*-methyl-Py_2TTAH]$^+$** cation and the methylene peak of the **[*S*-ethyl-Py_2TTAH]$^+$** cation are in close proximity. This is consistent with what is expected between methylene and methyl protons in an otherwise similar environment. Comparison of the ^{13}C NMR spectra also revealed many parallels with overlapping pyridyl peaks and

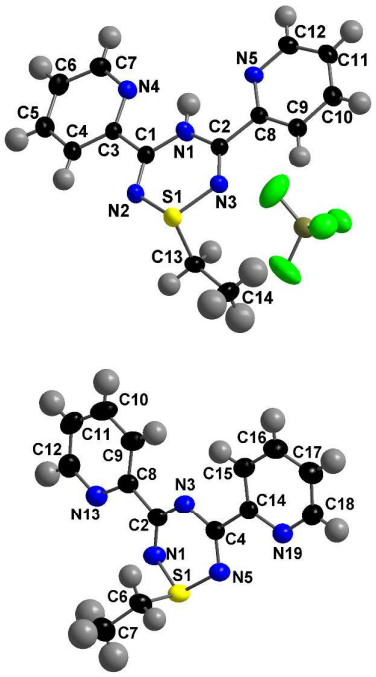

Fig. 1 50% thermal ellipsoid drawings of **[*S*-ethyl-Py_2TTAH][BF_4]** (top) and ***S*-ethyl-Py_2TTA** (bottom).

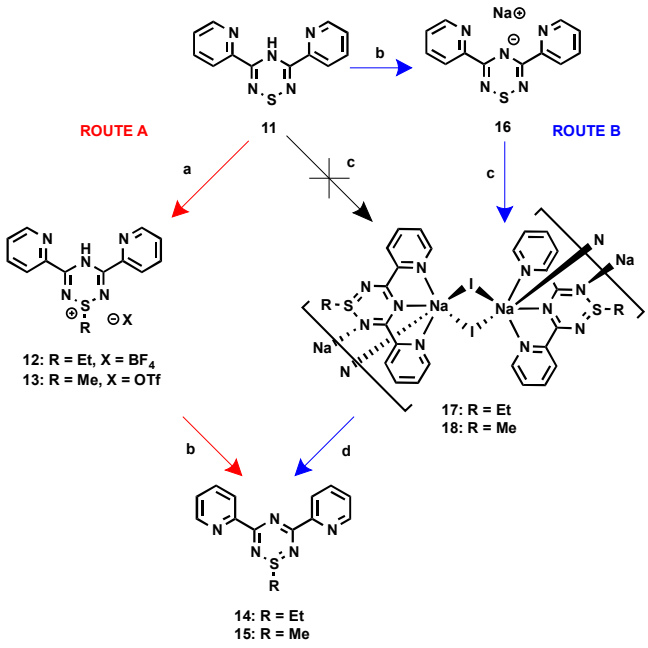

Scheme 1. Synthesis of *S*-alkyl-3,5-*bis*-(2-pyridyl)-1,2,4,6-thiatriazines. Reagents and conditions: (a) $[Et_3O][BF_4]$·DCM or MeOTf, DCM; (b) NaH, THF; (c) EtI or MeI, THF; (d) H_2O/DCM.

deshielded *S*-alkyl peaks (Figure S8 and S9). In addition, an upfield shift of 9 ppm for the methyl carbon can be observed in comparison to the methylene of **[*S*-ethyl-Py$_2$TTAH]**$^+$. Subsequent treatment of **13** with NaH in tetrahydrofuran (THF) affords ***S*-methyl-Py$_2$TTA** (**15**) as a dark yellow solid. Yellow needles of **15** can be obtained from recrystallization in a THF/hexanes mixture; however, crystals suitable for X-ray analysis remain elusive. Nonetheless, comparison of the IR and NMR spectra (Figure S5 and S11) with those of the ethyl derivative **14** (Figure S4 and S10) supports the identification of **15** as ***S*-methyl-Py$_2$TTA**.

Interestingly, upon inspection of the mother liquor removed from the reaction between **Py$_2$TTAH** and MeOTf, a minor side product was crystallized, which afforded different IR and NMR spectra compared to **[*S*-methyl-Py$_2$TTAH][OTf]** (Figures S1-S3). In addition to shifts in the pyridyl peaks, the ^{1}H NMR spectrum revealed two unique methyl singlets, which integrate in a 1:2 ratio, consistent with the preparation of the 3,5-*bis*(*N*-methyl-2-pyridinium)-*S*-methyl-1,2,4,6-thiatriazine dication. In order to confirm its identity, the yellow block-like crystals were studied *via* single crystal X-ray analysis. Crystals of **[3,5-*bis*(*N*-methyl-2-pyridinium)-*S*-methyl-1,2,4,6-thiatriazine][OTf]$_2$**, which belong to the triclinic space group $P\bar{1}$, confirm methylation occurred on both pyridyl substituents in addition to the sulphur atom in the TTA ring (Figure 2). The presence of two triflate anions in the asymmetric unit simply serves to balance the charge induced by the methylated pyridinium substituents. This, coupled with the uniformity of the C—N bond lengths in the TTA framework (Table S2), is indicative of a neutral aromatic thiatriazine moiety. Similar to ***S*-ethyl-Py$_2$TTA**, the six membered TTA ring also adopts a shallow boat-like conformation with the S1 and N3 atoms displaced from the mean plane of the remaining four atoms by 0.409(1) Å and 0.120(1) Å, respectively. As well, the pyridyl rings are twisted with respect to the TTA ring with torsion angles of 17.1(1)° and 49.5(1)° (Figure S15), which are greater than the twist angles observed in ***S*-ethyl-Py$_2$TTA**. This is likely due to the steric bulk introduced by the methyl substituents.

In addition to [Et$_3$O][BF$_4$] and MeOTf, alkyl iodides were also employed. To that end, methyl iodide (MeI) and ethyl iodide (EtI) were added to solutions of **Py$_2$TTAH** in both THF and DCM; however, no reaction occurred. To overcome this challenge, we considered deprotonation prior to alkylation; however, initial attempts to deprotonate **Py$_2$TTAH** using bases such as DMAP, proton sponge and KOH were unsuccessful.[20] Nevertheless, we recently demonstrated that **Py$_2$TTAH** is susceptible to deprotonation upon metal coordination (e.g., Fe).[11] Having established that deprotonation is possible, we therefore considered an irreversible base such as NaH to access the anionic derivative prior to alkylation with weaker alkylating agents. To that end, upon the treatment of **Py$_2$TTAH** with NaH in THF, H_2 gas evolved and the initial purple solution turned bright emerald green, indicative of deprotonation (i.e., formation of **16**). Subsequent treatment of **16** with EtI afforded a brown solution from which an air-stable orange solid slowly precipitated. Crystallization of this material through vapour diffusion of diethyl ether (Et_2O) into a saturated DCM solution afforded yellow block-like crystals suitable for X-ray analysis, confirming the structural identity of **17** as a coordination polymer with an *S*-ethyl-TTA ligand (Figure 2). More specifically, crystals of **17** belong to the triclinic space group $P\bar{1}$ and consist of dimeric units that are connected through a weak bond between the metal centre and a nitrogen atom on a neighbouring TTA ligand, leading to a 1D coordination polymer. The metal ion adopts a distorted six coordinate geometry with the sodium centre bound to the pincer-type ***S*-ethyl-Py$_2$TTA** ligand through three nitrogen atoms (N1, N2 and N3). Two additional iodide ions (I1 and I1a) are μ-bridging to the next sodium centre in the dimer, resulting in a diamond-like arrangement between the sodium and iodide ions in the plane perpendicular to the tridentate ***S*-ethyl-Py$_2$TTA** ligand. A weak Na—N bond from the N-S-N portion of a neighbouring TTA ring occupies the remaining coordination site, thus forming a 1D chain. The Na—N bond lengths (2.45-2.48 Å) as well as charge balance suggests the *S*-ethylated-TTA ligand is neutral. Dissolution of **17** into water followed by extraction with DCM afforded ***S*-ethyl-Py$_2$TTA** (**14**). This therefore demonstrates *S*-ethyl-TTA can be prepared *via* a cationic (Route A) or anionic (Route B) intermediate, as outlined in Scheme 1. While both routes are effective at generating **14**, Route B is superior in terms of enhanced yields (<10 % *vs*. >80%) and purity of the crude material. Furthermore, the reaction with alkyl iodides is more cost effective and less time consuming (>48 h *vs*. 20 h).

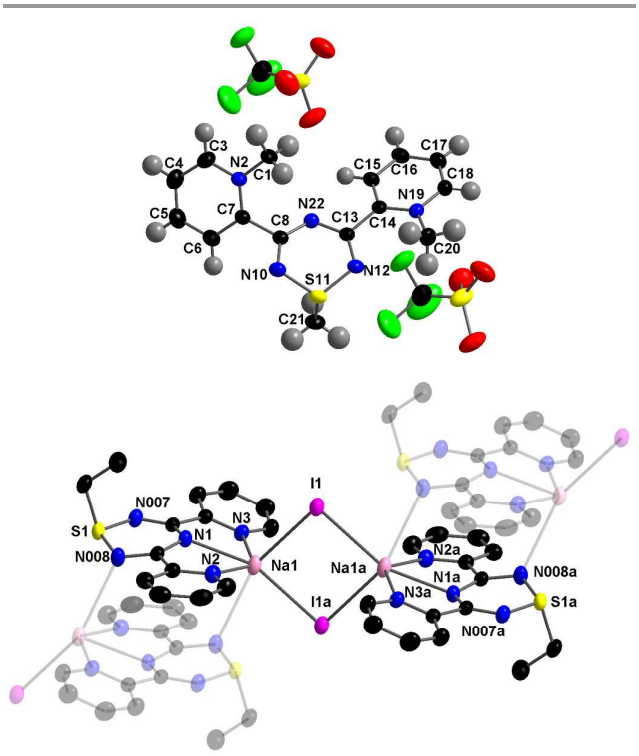

Fig. 2 50% thermal ellipsoid drawings of **[3,5-*bis*(*N*-methyl-2-pyridinium)-*S*-methyl-1,2,4,6-thiatriazine][OTf]$_2$** (top) and **17** (bottom). Hydrogen atoms omitted for clarity in the molecular structure of **17**.

Similarly, treatment of **16** with methyl iodide afforded **18** as a yellow precipitate. Recrystallization *via* vapour diffusion of Et_2O into a saturated solution of acetonitrile (MeCN) afforded pure material; however, despite our best efforts, crystals suitable for single X-ray analysis remain elusive. Nonetheless, comparison of the IR and NMR spectra with those of **17** revealed many similarities. For

example, the fingerprint regions of the IRs for the two compounds share many of the same peaks, albeit with slightly shifted frequencies. While **17** has more activity below 800 cm^{-1}, this is to be expected since C—H rocking bands in alkanes appear in this region and **17** has a greater quantity compared to **18**. The ^{1}H NMR spectra show identical pyridyl peaks in the aromatic region (8.6, 8.4, 8.0, and 7.6 ppm) for MeCN-d3 solutions of both compounds (Figure S6 and S7). As well, the methyl protons in **18** are shielded with respect to the methylene protons of **17**, with a small upfield shift of 0.37 ppm. Likewise, the ^{13}C NMR spectra for MeCN-d3 solutions of compounds **17** and **18** are almost identical, with the only difference being the small upfield shift of the methyl signal in **18** compared to the methylene of **17** (Figure S12 and S13). It should be noted in solution **17** and **18** are likely the dimeric species or some other discrete sodium-iodide adduct, not coordination polymers. Nonetheless, these results suggest that intermediate **18** is similar to **17**. Furthermore, subsequent aqueous treatment of **18** followed by extraction with DCM afforded a dark yellow solid that exhibits NMR spectra consistent with that of ***S*-methyl-Py_2TTA (15)**.

Theoretical and Spectroscopic Studies

The apparent regioselective alkylation observed here, that is, preferential *S*-aklylation, may be rationalized in terms of the orbital coefficients of the frontier molecular orbitals of the starting material (i.e. **Py_2TTAH**). DFT calculations using the B3LYP/6-311+G(2d,p) level of theory were performed on **11** (along with **14** and **15**); geometry optimized molecular orbitals and orbital energetics are provided in Table S3. In the description of the electronic structure of **Py_2TTAH,** the HOMO consists of two nodal planes bisecting the TTA ring through the S—N bonds and the C—N bonds opposite them with a significant portion of the electron density residing on the S atom. This may explain the regioselectivity as electrophilic addition tends to occur preferentially at the site whose frontier orbital has the largest coefficient. Interestingly, while slight variations in the relative energy levels are observed, the symmetry of the molecular orbitals of the alkylated derivatives (**14** and **15**) are similar to that of the starting material **Py_2TTAH**.

The photophysical properties of **14** and **15** were investigated and, although these compounds do not fluoresce, they absorb strongly in the UV-vis region of the electromagnetic spectrum (Figure 3). Perhaps unsurprisingly, the absorption profiles are superimposable, which further supports the assignment of **15** being the methylated derivative of **14**. The UV-vis spectra for both compounds are comprised of two main regions; one consisting of a weak, broad band centred near 390 nm and another containing intense bands absorbing at 200-300 nm. To probe the optical transitions, TD DFT calculations were performed on optimized geometries of **14** and **15**; the results of which are presented in Figure 3 and the twenty vertical excitation energies calculated for each compound are listed in Table S4. Overall, the predicted absorption profiles are in reasonable agreement with those experimentally obtained – i.e., the calculated maximum absorption wavelengths and relative intensities match the experimental behaviour well. The highest wavelength absorption, which is associated with the HOMO to LUMO transition, has relatively low oscillator strength (f = 0.0276 for **14**; f = 0.0273 for **15**). The band with the largest oscillator strength (f = 0.2499 and 0.2303 for **14** and **15**, respectively) corresponds to excitations arising from contributions of several transitions (see Tables S5 and S6). Furthermore, the oscillator strength predicted by computational methods correlates well with the measured molar extinction coefficients (see Table S7).

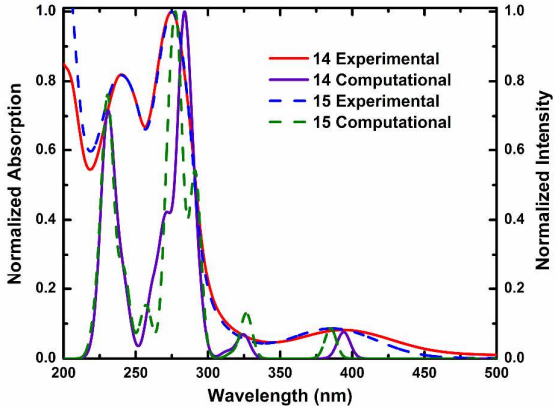

Fig. 3 Experimental absorption spectra of **14** (red solid line) and **15** (blue dashed line) in MeCN, as well as TD DFT calculated absorption spectra of **14** (purple solid line) and **15** (green dashed line).

Conclusions

To summarize, we have developed a flexible and general route for the preparation of *S*-alkyl-thiatriazines, which can proceed *via* two synthetic pathways; either through cationic (Route A) or anionic (Route B) intermediates. As it is expected that this methodology can be extended to the development of more complex examples, facile modification of the exocyclic substituents in thiatriazines may be achieved. Thus, the generation of a range of functionalized TTA derivatives can be anticipated. The work presented here is therefore an important finding, and holds potential in the design of novel heterocyclic compounds that can be targeted for applications ranging from mesogens in liquid crystalline materials to ionic liquids and electroactive substrates.

Taking advantage of the fact that alkylation occurs at the sulphur atom in the TTA ring, leaving the tridentate coordination pocket free to bond to a variety of metals, facilitates the development of novel ligand systems. To that end, linking two thiatriazines together *via* an alkyl tether would enable the development of coordination complexes that could easily be tailored by the choice of tether. A logical next step would involve the preparation of the pyrimidyl derivative, which would facilitate multimetallic coordination. Such a ligand system has significant potential towards the development of extended coordination polymers and networks. In conclusion, not only do we anticipate rich coordination chemistry for these *S*-alkyl-TTA derivatives acting as multidentate chelating ligands, we also foresee the development of novel heteroaromatic bridging ligands; such studies are currently underway.

Experimental Section

General procedures

The reagents sodium hydride (60% dispersion in mineral oil, Alfa Aesar) methyl iodide (Alfa Aesar), ethyl iodide (Sigma-Aldrich), triethyloxonium tetrafluoroborate (Sigma-Aldrich), and methyl trifluorosulfonate (methyl triflate, Synquest Labs Inc.) were obtained commercially and used as received. THF and DCM were dried by passing them through activated alumina on a J.C. Meyer solvent purification system and stored over 4Å Molecular sieves. All other solvents were reagent grade. 3,5-*bis*(2-pyridyl)-4-hydro-1,2,4,6-thiatriazine (**Py_2TTAH**)[28] was prepared as outlined in the literature. All reactions were performed under an atmosphere of dry nitrogen unless otherwise stated. Melting points were taken using a Mel-Temp apparatus and are uncorrected. ^{1}H NMR and ^{13}C NMR spectra were run in MeCN-d_3 solutions at room temperature on Bruker Avance 400 MHz or Bruker Avance 300 MHz spectrometers. IR spectra of solid samples were recorded on an Agilent Technologies Cary 630 FT-IR spectrometer. UV-visible spectra were measured using an Agilent Cary 5000 UV-Vis-NIR spectrophotometer in the range 200 – 1200 nm. Solution absorption measurements were completed using MeCN solutions with standard 10 mm pathlength cuvettes.

Crystal Growth

Bright yellow block-like crystals of **12** suitable for X-ray analysis were grown *via* slow evaporation of the reaction filtrate. Yellow needles of **14** suitable for X-ray analysis were grown through recrystallization from hexanes. Yellow block-like crystals of **[3,5-*bis*(*N*-methyl-2-pyridinium)-*S*-methyl-1,2,4,6-thiatriazine][OTf]$_2$** suitable for X-ray analysis were grown *via* vapour diffusion of chloroform into a saturated solution of acetone. Yellow blocks of **17** suitable for X-ray analysis were recrystallized *via* vapour diffusion of Et_2O into a saturated solution of DCM.

Crystallography

Data collection results for compounds **12**, **14, [3,5-*bis*(*N*-methyl-2-pyridinium)-*S*-methyl-1,2,4,6-thiatriazine][OTf]$_2$** and **17** represent the best data sets obtained in several trials for each sample. The crystals were mounted on thin glass fibers using paraffin oil. Prior to data collection crystals were cooled to 200(2) K (**12**, **[3,5-*bis*(*N*-methyl-2-pyridinium)-*S*-methyl-1,2,4,6-thiatriazine][OTf]$_2$**, **17**) and 258(2)K (**14**). Data was collected on Bruker AXS SMART and KAPPA single crystal diffractometers equipped with sealed Mo tube sources (wavelength 0.71073 Å) and APEX II CCD detectors. Raw data collection and processing was performed with the APEX II software package from BRUKER AXS.[29] Diffraction data for **12** and **17** were collected with a sequence of 0.3° ω scans at 0, 90, 180 and 270° in φ in order to ensure adequate data redundancy. Initial unit cell parameters were determined from 60 data frames with 0.3° ω scan each, collected at the different sections of the Ewald sphere. Diffraction data for **14** and **[3,5-*bis*(*N*-methyl-2-pyridinium)-*S*-methyl-1,2,4,6-thiatriazine][OTf]$_2$** were collected with a sequence of 0.5° ω and φ scans. Semi-empirical absorption corrections based on equivalent reflections were applied.[30] Systematic absences in the diffraction data-set and unit-cell parameters were consistent with triclinic $P\bar{1}$ (№2) for the **[3,5-*bis*(*N*-methyl-2-pyridinium)-*S*-methyl-1,2,4,6-thiatriazine][OTf]$_2$** and **17**, and orthorhombic $P2_12_12_1$ (№19) for **12** and **14**. Solutions in the centrosymmetric space groups for both **3,5-*bis*(*N*-methyl-2-pyridinium)-*S*-methyl-1,2,4,6-thiatriazine][OTf]$_2$** and **17** yielded chemically reasonable and computationally stable results of refinement. However, data for compounds **12** and **14** suggested non-centrosymmetric chiral space groups for the structural model. The structures were solved by direct methods, completed with difference Fourier synthesis, and refined with full-matrix least-squares procedures based on F^2.

Structural model of **12** consists of two oppositely charged fragments located in the general positions of the asymmetric unit. Refinement of the structure in the chiral space group settings yield -0.02(3) Flack x parameter, suggesting that a correct absolute structural configuration was chosen for the structural model.

For **14** the Flack x parameter is -0.05(3), which also supports the chosen absolute structural configuration.

The structural model of **3,5-*bis*(*N*-methyl-2-pyridinium)-*S*-methyl-1,2,4,6-thiatriazine][OTf]$_2$** indicated three charged fragments in the asymmetric unit, one dication and two anions. One of triflate anions was modelled as disordered over three positions with 0.435(1):0.435(1):0.131(2) occupancy ratio. Restraints, mainly for the S-C-F angle (S-F distance), C-F distance, and S-C distance were applied to make the molecule symmetrical and set its geometry equal for all three positions. 'Enhanced' rigid-bond restraints were also introduced for atom ADPs. Constraints for sulphur and oxygen atoms were applied, equalizing ADPs for the first two positions.

Solving structural model for **17** revealed one dimeric unit associated by two symmetry related iodine atoms I(1) and I(1A). Dimeric unit is located on one of the inversion centers of the space group.

Structural models were successfully refined with a full set of anisotropic thermal motion parameters for all non-hydrogen atoms. All hydrogen atom positions were calculated based on the geometry of related non-hydrogen atoms. All hydrogen atoms were treated as idealized contributions during the refinement. All scattering factors are contained in several versions of the SHELXTL program library, with the latest version used being v.6.12.[31]

Computational Chemistry

All calculations were carried out using the Gaussian09 program package.[32] The geometries of the studied compounds were investigated using the hybrid density functional B3LYP with the 6-311+G(2d,p) basis set. Optimized structures were used to examine the orbital energies and frontier molecular orbital probabilities. The calculated UV-vis spectra and excitation energies were determined using TD DFT which employed the optimized B3LYP ground states. The solvent model and solvent was MeCN, and twenty excited states were considered.

Synthetic Procedures

[*S*-ethyl-Py_2TTAH][BF_4] (12). Under an inert atmosphere, triethyloxonium tetrafluoroborate (78 mg, 0.411 mmol) was added to a solution of **Py_2TTAH** (0.1 g, 0.391 mmol) in DCM (10 mL). After 24 hours, the resulting mixture was filtered. Upon slow evaporation of the purple filtrate, large yellow crystals suitable for XRD were obtained, which crystallized alongside starting material. The yellow crystals were washed with DCM to remove the unreacted starting material. Yield 0.026 g (0.07 mmol, 18%) Dec. > 193°C. ^{1}H NMR (δ, MeCN-d3): 12.30 (1H, br), 8.85 (2H, ddd, J = 4.8, 1.5, 0.9 Hz, Ar), 8.34 (2H, ddd, J = 7.9, 1.1, 1.0 Hz, Ar), 8.14 (2H, ddd, J = 7.8, 7.7, 1.7 Hz, Ar), 7.82 (2H, ddd, J = 7.7, 4.8, 1.1 Hz, Ar), 3.71 (2H, q, J = 7.3 Hz), 1.53 (3H, t, J = 7.3 Hz). ^{13}C NMR (δ, MeCN-d3): 158.54, 150.57, 145.61, 139.96, 130.77, 124.48, 49.47, 5.89. IR ν_{max} (cm^{-1}): 3271 (m), 3059 (w), 2986 (w), 2940 (w), 2923 (w), 2852 (w), 1661 (s), 1638 (m), 1617 (w), 1585 (m), 1571 (m), 1560 (s), 1541 (m), 1534 (m), 1508 (w), 1470 (m), 1460 (s), 1451 (s), 1419 (s), 1395 (s), 1383 (s), 1357 (m), 1305 (w), 1285 (w), 1257 (w), 1161 (w), 1086 (m), 1063 (s), 1048 (s), 1031 (s), 1005 (s), 996 (s), 809 (m), 798 (s), 766 (m), 738 (s), 697 (s).

***S*-ethyl-Py_2TTA (14) *via* route A**. Under an inert atmosphere, 60% sodium hydride (0.0169 g, 0.424 mmol) was added to a stirring slurry of **12** (0.150 g, 0.404 mmol) in THF (10 mL). After 16 hours, then reaction mixture was quenched with water, extracted into DCM, dried over $MgSO_4$, filtered and the solvent removed under reduced pressure. The resulting yellow residue was dried *in vacuo* (yield 0.11g, 0.388 mmol, 96%). Recrystallization from hexanes afforded pure yellow crystals suitable for X-ray analysis. MP: 125-126°C. ^{1}H NMR (δ, MeCN-d3): 8.72 (2H, ddd, J = 4.7, 1.8, 0.9 Hz, Ar), 8.39 (2H, ddd, J = 7.9, 1.2, 0.9 Hz, Ar), 7.91 (2H, ddd, J = 7.9, 7.6, 1.8 Hz, Ar), 7.50 (2H, ddd, J = 7.6, 4.7, 1.3 Hz, Ar), 3.13 (2H, q, J = 7.5), 1.32 (3H, t, J = 7.4). ^{13}C NMR (δ, MeCN-d3): 171.68, 155.49, 150.41, 137.67, 126.99, 124.65, 45.54, 5.99. IR ν_{max} (cm^{-1}): 3051 (w), 3011 (w), 2965 (w), 2952 (w), 2922 (w), 2907 (w), 1574 (w), 1513 (m), 1451 (w), 1437 (w), 1424 (w), 1396 (s), 1379 (s), 1374 (s), 1332 (s), 1285 (m), 1250 (s), 1174 (m), 1112 (m), 1080 (w), 1053 (w), 1043 (m), 1022 (m), 994 (m), 968 (m), 910 (w), 898 (w), 841 (w), 822 (m), 812 (w), 793 (m), 775 (s), 752 (s), 737 (s), 725 (s), 693 (m), 681 (m), 674 (w), 669 (w), 660 (w), 655 (w).

[*S*-methyl-Py_2TTAH][OTf] (13). Under an inert atmosphere, methyl triflate (0.169 g, 1.03 mmol) was added to a solution of **Py_2TTAH** (0.25 g, 0.979 mmol) in DCM (15 mL). After 24 hours, **13** was filtered off, washed with DCM, and dried under reduced pressure. Yield: 0.3757 g (0.895 mmol, 91.5%). Dec. > 221**°C**. ^{1}H NMR (δ, MeCN-d3): 12.37 (1H, br), 8.86 (2H, ddd, J = 4.8, 1.7, 1.0 Hz, Ar), 8.33 (2H, ddd, J = 7.8, 1.1, 1.0 Hz, Ar), 8.14 (2H, ddd, J = 7.8, 7.7, 1.6 Hz, Ar), 7.82 (2H, ddd, J = 7.7, 4.8, 1.2 Hz, Ar), 3.43 (3H, s). ^{13}C NMR (δ, MeCN-d3): 158.16, 150.60, 145.68, 139.91, 130.77, 124.42, 40.45. IR ν_{max} (cm^{-1}): 3237 (m), 2991 (m), 2905 (m), 1651 (s), 1585 (m), 1572 (m), 1560 (s), 1463 (s), 1450 (m), 1406 (s), 1354 (w), 1313 (w), 1297 (w), 1251 (s), 1226 (s), 1169 (s), 1145 (s), 1092 (m), 1043 (w), 1029 (s), 1010 (m), 998 (s), 944 (w), 910 (w), 805 (m), 768 (m), 758 (w), 741 (s), 705 (s), 692 (s), 672 (w), 660 (w).

***S*-methyl-Py_2TTA (15) *via* route A.** Under an inert atmosphere, 60% sodium hydride (0.015 g, 0.375 mmol) was added to a stirring slurry of **13** (0.150 g, 0.358 mmol) in THF (5 mL). After 16 hours, then reaction mixture was quenched with water, extracted into DCM, dried over $MgSO_4$, filtered and the solvent removed under reduced pressure. The resulting yellow residue was dried *in vacuo* (yield 0.051g, 0.188 mmol, 52%). Solvent/antisolvent recrystallization with THF/hexanes afforded pure yellow needles. MP: 146-147°C. ^{1}H NMR (δ, MeCN-d3): 8.71 (2H, ddd, J = 4.7, 1.8, 0.9 Hz, Ar), 8.42 (2H, ddd, J = 7.9, 1.2, 0.9 Hz, Ar), 7.91 (2H, ddd, J = 7.9, 7.6, 1.8 Hz, Ar), 7.50 (2H, ddd, J = 7.6, 4.7, 1.2 Hz, Ar), 2.76 (3H, s). ^{13}C NMR (δ, MeCN-d3): 171.31, 155.47, 150.41, 137.70, 127.01, 124.74, 34.78. IR ν_{max} (cm^{-1}): 3048 (w), 2983 (w), 2899 (w), 1583 (w), 1502 (s), 1458 (m), 1438 (m), 1414 (m), 1375 (s), 1348 (m), 1327 (s), 1296 (m), 1282 (m), 1250 (m), 1141 (w), 1108 (m), 1188 (w), 1041 (w), 994 (m), 989 (m), 902 (w), 845 (w), 826 (w), 815 (w), 771 (m), 755 (s), 733 (m), 698 (m), 664 (w).

17. Under an inert atmosphere, 60% sodium hydride (0.164 g, 4.11 mmol) was added to a solution of **Py_2TTAH** (1 g, 3.92 mmol) in THF (25 mL), resulting in the evolution of hydrogen gas and a dark green solution. After 30 minutes, ethyl iodide (1.22 g, 7.83 mmol) was added and, after stirring for 17 hours, the resulting orange precipitate was filtered and dried in air. Yield 1.22 g (2.82 mmol, 72%). Yellow blocks suitable for X-ray analysis were recrystallized by vapour diffusion of Et_2O into a saturated solution of DCM. Dec. > 150°C. ^{1}H NMR (δ, MeCN-d3): 8.56 (2H, ddd, J = 4.8, 1.7, 0.9 Hz, Ar), 8.40 (2H, ddd, J = 8.0, 1.1, 1.0 Hz, Ar), 7.98 (2H, ddd, J = 8.0, 7.6, 1.7 Hz, Ar), 7.55 (2H, ddd, J = 7.6, 4.8, 1.2 Hz, Ar), 3.23 (2H, q, J = 7.4 Hz), 1.37 (3H, t, J = 7.5 Hz). ^{13}C NMR (δ, MeCN-d3): 170.50, 153.85, 150.24, 138.99, 128.09, 124.86, 46.89, 5.81. IR ν_{max} (cm^{-1}): 3047 (w), 1587 (w), 1571 (w), 1529 (s), 1467 (w), 1437 (m), 1396 (w), 1375 (s), 1352 (m), 1335 (s), 1287 (m), 1268 (w), 1257 (m), 1145 (m), 1086 (m), 1048 (m), 1001 (s), 903 (w), 837 (w), 822 (m), 775 (s), 761 (s), 746 (s), 725 (s), 716 (m), 710 (w), 705 (w), 700 (w), 695 (s), 690 (m), 685 (m), 681 (m), 675 (w) , 670 (m), 665 (m), 660 (m), 655 (m).

***S*-ethyl-Py_2TTA (14) *via* route B**. **17** (1.19g, 2.74 mmol) was dissolved in a water/THF mixture (7:3), extracted into DCM, dried over $MgSO_4$, filtered and the solvent removed under reduced pressure. The resulting brown residue was dried *in vacuo.* Solvent/antisolvent recrystallization with DCM/hexanes afforded **14** as pure yellow crystals (yield 0.75 g, 2.65 mmol, 96%). Spectroscopic data were identical to those for material prepared *via* route A.

18. Under an inert atmosphere, 60% sodium hydride (0.164 g, 4.11 mmol) was added to a solution of **Py_2TTAH** (1 g, 3.92 mmol) in THF (20 mL), resulting in the evolution of hydrogen gas and a dark green solution. After 30 minutes, methyl iodide (1.11 g, 7.83 mmol) was added and, after stirring for 16 hours, the resulting yellow precipitate was filtered and dried in air. Yield 1.38 g (3.30 mmol, 84%). Pure material was obtained by

vapour diffusion of Et_2O into a saturated solution of MeCN. Dec. > 155°C. ^{1}H NMR (δ, MeCN-d3): 8.56 (2H, ddd, J = 4.8, 1.7, 0.9 Hz, Ar), 8.41 (2H, ddd, J = 7.8, 1.1, 1.0 Hz, Ar), 7.99 (2H, ddd, J = 7.8, 7.7, 1.7 Hz, Ar), 7.56 (2H, ddd, J = 7.6, 4.8, 1.2 Hz, Ar), 2.86 (3H, s). ^{13}C NMR (δ, MeCN-d3): 170.32, 154.01, 150.30, 139.03, 128.12, 124.94, 35.96. IR ν_{max} (cm^{-1}): 3049 (w), 3008 (w), 1588 (w), 1575 (w), 1528 (m), 1504 (m), 1442 (w), 1431 (w), 1399 (m), 1379 (s), 1333 (m), 1292 (m), 1253 (m), 1177 (w), 1146 (w), 1115 (m), 1090 (w), 1051 (w), 1044 (m), 1016 (w), 1002 (m), 983 (m), 938 (w), 911 (w), 843 (w), 828 (w), 791 (s), 757 (s), 728 (s), 699 (m), 669 (w).

***S*-methyl-Py$_2$TTA (15) *via* route B**. **18** (1.33 g, 3.17 mmol) was dissolved in a water/THF mixture (7:3), extracted into DCM, dried over $MgSO_4$, filtered and the solvent removed under reduced pressure. The resulting dark yellow residue was dried *in vacuo*. Solvent/antisolvent recrystallization with THF/hexanes afforded **15** as pure yellow needles (yield 0.85 g, 3.14 mmol, 99%). Spectroscopic data were identical to those for material prepared *via* route A.

Acknowledgements

This work was supported by the University of Ottawa, the Canadian Foundation for Innovation, the National Sciences and Engineering Council of Canada and the Ontario Research Fund. J.L.B. is grateful to the Ontario Ministry of Research and Innovation for an Early Researcher Award.

Notes and References

1. C. Wang, H. Dong, W. Hu, Y. Liu and D. Zhu, *Chem. Rev.*, 2012, **112**, 1083-1088.
2. M. P. Cava, M. V. Lakshmikantham, R. Hoffmann and R. M. Williams, *Tetrahedron*, 2011, **67**, 6771-6797.
3. M. E. Cinar and T. Ozturk, *Chem. Rev.*, 2015, **115**, 3036-3140.
4. B. F. Abdel-Wahab and S. Shaaban, *Synthesis-Stuttgart*, 2014, **46**, 1709-1716.
5. F. A. Davis, *J. Org. Chem.*, 2006, **71**, 8993-9003.
6. A. K. Boudalis, C. P. Raptopoulou, A. Terzis and S. P. Perlepes, *Polyhedron*, 2004, **23**, 1271-1277.
7. A. W. Cordes, P. J. Hayes, P. D. Josephy, H. Koenig, R. T. Oakley and W. T. Pennington, *Chem. Comm.,* 1984, 1021-1022.
8. P. J. Hayes, R. T. Oakley, A. W. Cordes and W. T. Pennington, *J. Am. Chem. Soc.*, 1985, **107**, 1346-1351.
9. R. T. Boere, R. T. Oakley, R. W. Reed and N. P. C. Westwood, *Journal of the American Chemical Society*, 1989, **111**, 1180-1185.
10. R. T. Boere, R. T. Oakley, R. W. Reed and N. P. C. Westwood, *J. Am. Chem. Soc.*, 1989, **111**, 1180-1185.
11. K. L. M. Harriman, A. A. Leitch, S. A. Stoian, F. Habib, J. L. Kneebone, S. I. Gorelsky, I. Korobkov, S. Desgreniers, M. L. Neidig, S. Hill, M. Murugesu and J. L. Brusso, *Dalton Trans.*, 2015, **44**, 10516-10523.
12. C. Y. Ang, R. T. Boere, L. Y. Goh, L. L. Koh, S. L. Kuan, G. K. Tan and X. Yu, *Chem. Comm.*, 2006, 4735-4737.
13. C. Y. Ang, S. L. Kuan, G. K. Tan, L. Y. Goh, T. L. Roemmele, X. Yu and R. T. Boere, *Can. J. Chem.*, 2015, **93**, 181-195.
14. N. J. Yutronkie, I. A. Kühne, I. Korobkov, J. L. Brusso and M. Murugesu, *Chemical Communications*, 2016, **52**, 677-680.
15. R. T. Boere, A. W. Cordes, P. J. Hayes, R. T. Oakley, R. W. Reed and W. T. Pennington, *Inorg. Chem.*, 1986, **25**, 2445-2450.
16. WO Pat., 9808845-A1, 1998.
17. WO Pat., 9725319-A, 1997.
18. WO Pat., 9725318-A, 1997.
19. L. C. Peng, F. Xiang, E. Roberts, Y. Kawagoe, L. C. Greve, K. Kreuz and D. P. Delmer, *Plant Physiol.*, 2001, **126**, 981-992.
20. N. J. Yutronkie, A. A. Leitch, I. Korobkov and J. L. Brusso, *Cryst. Growth Des.*, 2015, **15**, 2524-2532.
21. M. Haake, H. Fode and K. Ahrens, *Z. Naturforsch. B*, 1973, **B 28**, 539-540.
22. J. Goerdeler and D. Loevenich, *Chem. Ber-Recl.*, 1954, **87**, 1079-1082.
23. J. Goerdeler and B. Wedekind, *Chem. Ber-Recl.*, 1962, **95**, 147-153.
24. W. Ried and M. A. Jacobi, *Chem. Ber-Recl.*, 1988, **121**, 383-386.
25. R. Appel and G. Vollmer, *Chem. Ber-Recl.*, 1970, **103**, 2555-2561.
26. Y. G. Shermolovich, V. S. Talanov, V. V. Pirozhenko and L. N. Markovskii, *Zh. Org. Khim.*, 1982, **18**, 2539-2547.
27. A. D. Stoller, *J. Het. Chem.*, 2000, **37**, 583-595.
28. A. A. Leitch, I. Korobkov, A. Assoud and J. L. Brusso, *Chem. Comm.*, 2014, **50**, 4934-4936.
29. APEX Software Suite and W. Bruker AXS: Madison, 2005.
30. R. H. Blessing, *Acta Crystallogr. Sect. A*, 1995, **51**, 33-38.
31. G. M. Sheldrick, *Acta Crystallogr. Sect. A*, 2008, **64**, 112-122.
32. M. J. Frisch, G. W. Trucks, H. B. Schlegel, G. E. Scuseria, M. A. Robb, J. R. Cheeseman, G. Scalmani, V. Barone, B. Mennucci, G. A. Petersson, H. Nakatsuji, M. Caricato, X. Li, H. P. Hratchian, A. F. Izmaylov, J. Bloino, G. Zheng, J. L. Sonnenberg, M. Hada, M. Ehara, K. Toyota, R. Fukuda, J. Hasegawa, M. Ishida, T. Nakajima, Y. Honda, O. Kitao, H. Nakai, T. Vreven, J. A. Montgomery, Jr., J. E. Peralta, F. Ogliaro, M. Bearpark, J. J. Heyd, E. Brothers, K. N. Kudin, V. N. Staroverov, R. Kobayashi, J. Normand, K. Raghavachari, A. Rendell, J. C. Burant, S. S. Iyengar, J. Tomasi, M. Cossi, N. Rega, J. M. Millam, M. Klene, J. E. Knox, J. B. Cross, V. Bakken, C. Adamo, J. Jaramillo, R. Gomperts, R. E. Stratmann, O. Yazyev, A. J. Austin, R. Cammi, C. Pomelli, J. W. Ochterski, R. L. Martin, K. Morokuma, V. G. Zakrzewski, G. A. Voth, P. Salvador, J. J. Dannenberg, S. Dapprich, A. D. Daniels, Ö. Farkas, J. B. Foresman, J. V. Ortiz, J. Cioslowski and D. J. G. Fox, Gaussian 09, Revision A.02; Gaussian, Inc.: Wallingford CT, 2009.

Graphical Abstract

Alkyl-functionalization of 3,5-*bis*(2-pyridyl)-1,2,4,6-thiatriazine

Elizabeth Kleisath, [a,b] *Nathan J. Yutronkie, Ilia Korobkov,* [a] *Bulat M. Gabidullin*[a] *and Jaclyn L. Brusso** [a,b]

[a] Department of Chemistry and Biomolecular Sciences [b] Centre for Catalysis Research and Innovation, University of Ottawa, Ottawa, Ontario K1N 6N5, Canada.

S-alkyl-1,2,4,6-thiatriazines, which can be prepared *via* two pathways, are described. The regioselectivity and photophyscial properties are rationalized through computational studies.